Indoor Office Channel Measurements and Analysis of Propagation Characteristics at 14 GHz

Runquan Miao*, Lei Tian*, Yi Zheng†, Pan Tang*, Fusheng Huang*, Jianhua Zhang*
*Beijing University of Posts and Telecommunications, Beijing, China
†China Mobile Research Institute, Beijing, China
Email: {miaorunquan, tianlbupt, tangpan27, huangfs, jhzhang}@bupt.edu.cn
zhengyi@chinamobile.com

***Abstract*—In this paper, we present the small scale characteristics of indoor office scenario based on the channel measurement at 14 GHz with 250 MHz bandwidth. The measurements were operated at more than 100 receiver locations including LOS and NLOS cases over distances up to 55 meters by utilizing a sliding correlator sounder with 125 mega-chip per second (Mcps). Besides, highly directional horn antennas and dipole antennas were used, respectively, to get the channel characteristics including power delay profile (PDP), path number and root-mean-square (rms) delay spread. The results of path number and rms delay spread measured by dipole antennas and horn antennas are different in LOS case. Compared with the results measured by horn antennas, the path number and rms delay spread value obtained by dipole antennas is bigger in LOS case, where rms delay spread values are 30 ns and 52 ns, respectively. It is reasonable that some multipath information is lost when using horn antenna to measure. In NLOS case, path number and rms delay spread only measured by dipole antennas are given.**

I. Introduction

As the development of smart phone and mobile application, mobile traffic has experienced a explosive increase. Specially, [1] makes a prediction that the mobile traffic will grow more than 1000 times in the next 10 years. It is also predictable that spectrum below 6 GHz will be crowded absolutely. To alleviate this problem, new technologies [2] and bands need to be used. Moreover, there has been growing interest in high frequency bands above 6 GHz [3]–[5]. Because high frequency bands can not only provide much more spectrum, but also make antennas' size smaller, which also helps realize massive Multiple-Input Multiple-Output (MIMO) application.

Though utilizing high frequency bands has apparent benefits, there are many problems needed to be considered, such as the cost of mass-producing chips and high free-space path loss [6]. Especially, path loss at high frequency bands will be higher, which significantly influences the design of cellular network. Thus, extensive measurements at high frequency bands are necessary [6]. [7] presents the large scale parameters of wideband multipath channels based on extensive measurement campaigns at 11 GHz. [8] describes an indoor channel measurement system at 28 GHz and gives analysis result of propagation characteristcs. Moreover, New York University (NYU) has done many measurements at 28 GHz [9], 38 GHz and 60 GHz [10], [11]. All of these measurements give some insights on channel characteristics at high frequency band, such as path loss and rms delay spread.

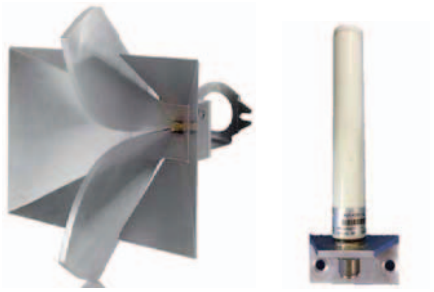

(a) horn antenna (b) dipole antenna

Fig. 1. Horn antenna and dipole antenna

Because of the comparative low path loss and wide available band (14 GHz - 15.3 GHz can be used for mobile communication in China), 14 GHz may be used as carrier frequency in the next generation wireless communication system. In this paper, we lay emphasis on investigating the propagation characteristics of indoor office radio channel based on our channel measurements at 14 GHz. Besides, high frequency is more likely to be used at a small range of distance, so we choose office as measurement scenario. A long-standing obstacle for the realization of millimeter waves systems is the high free-space path loss, so the high-gain (high directivity) antennas are widely used to compensate the path loss [10]–[15]. During our measurements, two kinds of antennas, highly directional horn antenna as Fig. 1(a) and dipole antenna as Fig. 1(b), are utilized respectively at the same measurement spots where are line-of-sight (LOS). Besides, we also use dipole antenna to conduct measurement in non line-of-sight (NLOS) environment. PDP, path number and delay information with different antennas are obtained and we make a comparison with them. All of these efforts will help to character propagation channel in indoor office scenario at 14 GHz.

The remainder of this paper is organized as follows. The measurement system and scenario are explained in Section II. Data processing methods are described in Section III. Results and analysis of propagation parameters are discussed in Section IV. Section V summarizes the results of our work and concludes this paper.

978-1-4673-6782-0/15/$31.00 ©2015 IEEE

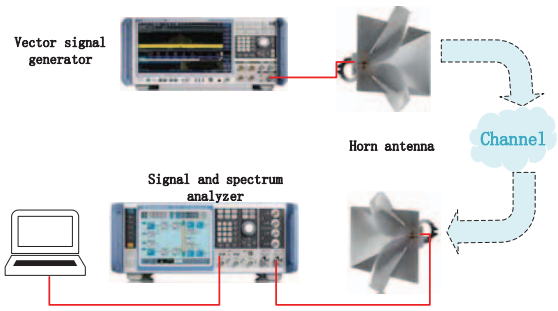

Fig. 2. The structure of 14 GHz measurement platform.

II. Measurement Description

A. Measurement System

The measurement platform in our measurements is mainly make up of instruments of Rohde & Schwarz as Fig. 2. We use R&S®SMW200A vector signal generator as transmitter at the Tx side, whose frequency ranges from 100 KHz to 20 GHz. Besides, the transmitted power before Tx antenna can be up to +30 dBm, which guarantees long enough measurement distance for indoor office scenario. At the Rx side, R&S®FSW signal and spectrum analyzer is utilized and its maximum analysis bandwidth can be 320 MHz.

In our measurement campaign, the center frequency of transmitter is set to 14 GHz with 250 MHz bandwidth and the PN sequence whose length is 2^{16} are transmitted at a rate of 125 Mcps. Thus, this platform allows a multipath time resolution of 4 ns (double sampling) and the total time of a PN sequence is 524 us (about 0.5 ms). For 14 GHz, if we assume the maximal moving speed v is 1 m/s, the channel coherence time calculated by

$$T_c \approx \frac{1}{f_m} = \frac{c}{vf} \tag{1}$$

is about 21 ms, where f_m is the maximal Doppler frequency and c is the velocity of light. The calculate result shows that we can obtain a complete sample in the coherence time. Besides, a total of 228 samples (snapshots) were obtained at each measurement spot. Double-ridged waveguide horn antennas and dipole antennas as Fig. 1 are used separately. The basic parameters of these two kinds of antennas are listed in Table I. Where E and A indicate the angle of elevation and azimuth, respectively.

TABLE I
ANTENNA PARAMETERS

	Horn antenna	dipole antenna
Frequency range [GHz]	0.8 to 18	13 to 15
Polarization	vertical	vertical
Gain [dBi]	14.1	1.5
3dB beam width(E)	$-18° \sim 18°$	$-30° \sim 30°$
3dB beam width(A)	$-16° \sim 16°$	$-180° \sim 180°$

B. Measurement Scenario

The channel measurement campaign is carried out on the 21th floor of the Innovation Building in China Mobile Research Institute. We had executed two different measurements, respectively, illustrated by Fig. 3.

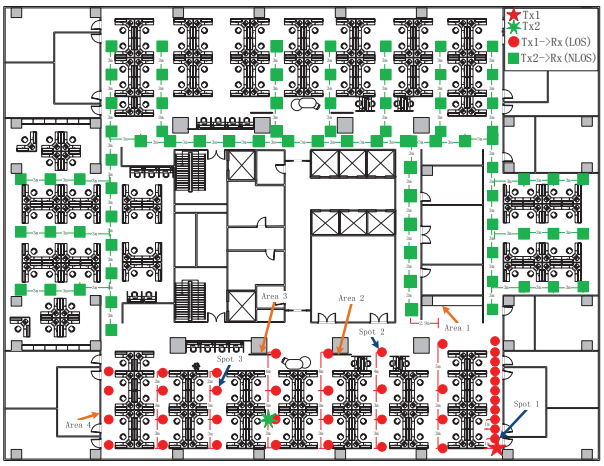

Fig. 3. Layout of the measurement

In our measurements, the transmitter (Tx) is installed in the corner and at the center of modern office, respectively. We both use dipole antenna and horn antenna to measure for LOS case (represented by red circular dots) when the transmitter is set up in the corner (represented by red five-pointed star) and only use dipole for NLOS case (represented by green square dots) when the transmitter is installed at the center (represented by green seven-pointed star). The measurement spots where receiver (Rx) are installed are mainly planned in corridor between different workstations or rooms. The distance range is 1 - 40 m in LOS case and 18 - 47 m in NLOS case, respectively.

III. Data Processing Methods

A. PDP

The measured channel impulse response (CIR) can be modeled as $h(\tau_l), l = 1, 2, \cdots, L$, where τ_l indicates the delay of the lth sample in the delay domain. L is the sampling length of a CIR at certain time. Then the power delay profile (PDP) corresponding to the CIR can be calculated by

$$P(\tau_l) = \|h(\tau_l)\|^2, l = 1, 2, \cdots, L \tag{2}$$

where $\|\cdot\|$ indicates 2-norm operation.

Power delay profile reveals the power strength of received signal and travel time of arrived resolvable paths.

B. Path Number

The number of the paths of a CIR snapshot equals to the number of extremum values of the power delay profile.

Firstly, we define the sub-paths as a set of all the valid sampling values of the CIR snapshot. Based on the definition

of the CIR before, the sub-path of the CIR can be further defined by

$$\mathcal{A} = h(\tau_l)|P(\tau_l) > X_s, l = 1, 2, \cdots, L, \tag{3}$$

where X_s is a empirical threshold which is related to the noise level of the CIR. We have two different methods to set X_s, and we called them M_1 and M_2, respectively. The methods are described as follows:

•M_1: Determine the threshold X_s according to the dynamic range and average power of the noise. The dynamic range of noise is obtained by a large number of samples. This method can get more effective samples when SNR is low.

•M_2: Determine the threshold X_s according to the dynamic range and peak power of the signal. The threshold is set to the value when multipath energy falls to X dB below the peak power of the signal. When the dynamic range of the sample is smaller than or close to X dB, the sample will be rejected.

For ease of analysis, we define $\mathcal{U} = \{\tau_l|h(\tau_l) \in \mathcal{A}, l = 1, 2, \cdots, L\}$. Then the extremum values set of the power delay profile can be denoted by

$$\mathcal{B} = \{P(\tau_l)|P(\tau_l) > P(\tau_{l-1}), P(\tau_l) > P(\tau_{l+1}), \tau_l \in \mathcal{U}\} \tag{4}$$

Thereby, the path number of the CIR is the element number of $\mathcal{B}$.

C. delay

The mean excess delay, rms delay spread and maximum excess delay (X dB) are multipath channel parameters that can be determined from a power delay profile. The time dispersive properties of wide band multipath channels are most commonly quantified by their mean excess delay ($\bar{\tau}$) and rms delay spread (σ_τ). First of all, we give the definition of each parameter based on [16].

The rms delay spread is the square root of the second central moment of the power delay profile. So the rms delay spread can be simply calculated by

$$\sigma_\tau = \sqrt{\bar{\tau^2} - (\bar{\tau})^2} \tag{5}$$

where the bar over the variable means doing the average operation, $\bar{\tau^2}$ and $\bar{\tau}$ can be calculated by

$$\bar{\tau^2} = \frac{\sum\limits_{\tau_l \in \mathcal{U}} P(\tau_l)\tau_l^2}{\sum\limits_{\tau_l \in \mathcal{U}} P(\tau_l)} \tag{6}$$

and

$$\bar{\tau} = \frac{\sum\limits_{\tau_l \in \mathcal{U}} P(\tau_l)\tau_l}{\sum\limits_{\tau_l \in \mathcal{U}} P(\tau_l)} \tag{7}$$

These delays are measured relative to the first detectable signal arriving at the receiver at $\tau_0 = 0$. Equations (6) and (7) do not rely on the absolute power level of $P(\tau)$, but only the relative amplitudes of the multipath components within $P(\tau)$.

The maximum excess delay (X dB) of the power delay profile is defined to be the time delay during which multipath energy falls to X dB below the maximum. In other words, the maximum excess delay is defined as $\tau_X - \tau_0$, where τ_0 is the first arriving signal and τ_X is the maximum delay at which a multipath component is within X dB of the strongest arriving multipath signal (which does not necessarily arrive at τ_0).

IV. Results Analysis

A. PDP

We mainly compare the PDPs measured by horn antennas and dipole antennas. For easy of comparison, we set the peak value of power to 0 dB, then the average noise power will be different because the SNRs of received signal measured by different types of antennas are not same.

To distinguish the different paths, we can calculate the difference of propagation distance, at least 1.2 m. Because the delay resolution of this platform is 4 ns. Besides, by analyzing PDP, we can get the propagation distance difference compared to the main path (generally direct path in LOS case). Fig. 4 - Fig. 6 show the PDPs when the Rx is installed at spot 1, spot 2 and spot 3 as shown in Fig. 3, respectively. During calculating path numbers, X is set to 20 dB.

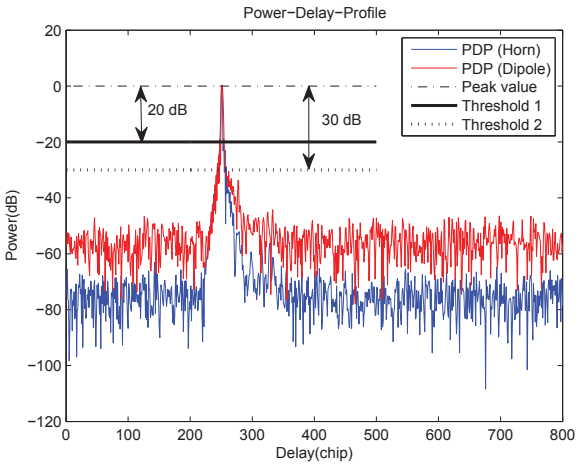

Fig. 4. The PDP when Rx is installed at spot 1

Fig. 4 shows that the numbers of effective paths measured by horn antennas and dipole antennas are both 1 at spot 1 (Tx - Rx distance is 1 m). And we can find that there is not the condition that can form strong, separable paths through observing the surrounding environment of spot 1.

Fig. 5 shows that the numbers of effective paths measured by horn antennas and dipole antennas are 1 and 9 at spot 2 (Tx - Rx distance is 15 m), respectively. The propagation distance difference between the obvious separable path in circles (shown in Fig. 5) and the main path is about 5 m. The path is most likely reflect to the Rx though area 1 in Fig. 3.

Fig. 6 shows that the numbers of effective paths measured by horn antennas and dipole antennas are 1 and 5 at spot 3 (Tx - Rx distance is about 30 m), respectively. The propagation distance differences are 7.2 m, 10.8 m, 22.8 m, 32.4 m and

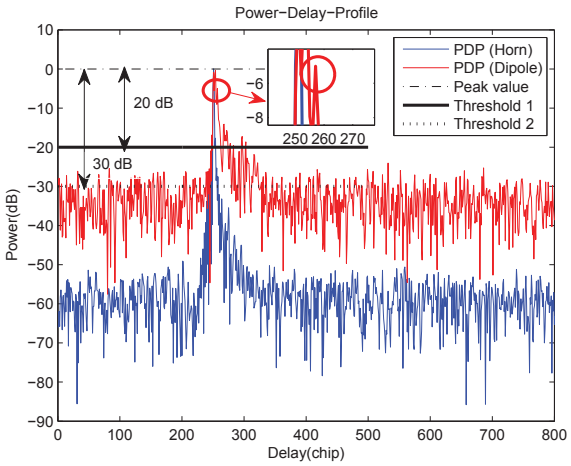

Fig. 5. The PDP when Rx is installed at spot 2

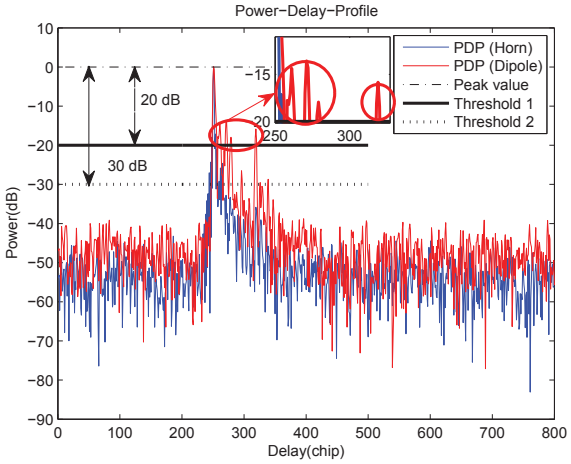

Fig. 6. The PDP when Rx is installed in spot 4

80.4 m. The first four paths most likely come from area 2, area 3 and area 4 in Fig. 3. The last one path may be the product of multiple reflections, or the synthetic results of some paths with similar delay.

From the above three figures, we find that the path number measured by dipole horn antennas is less than that measured by dipole antennas. This is because of the high directivity of horn antennas. Besides, we find that non-direct paths have much smaller energy compared to direct paths, especially when the SNR is high. When we calculate rms delay spread, the most weak paths have little influence on the result.

B. Path Number

Table II shows the mean path numbers of different cases in our measurements, and some samples with low SNR are not considered during calculating the path numbers.

It can be seen from Table II that the mean path number measured by horn antennas is more than that measured by dipole antennas in LOS case when we use M_1 to extract the paths. Investigating its reason, signal-noise-ratio (SNR) is a factor that can not be neglected. The received signal have high SNR, which results in more paths captured when we use horn antennas in the received scope of the antenna. In contrast, the low SNR gives rise to many paths submerged in noise, and can not be separated.

TABLE II
PATH NUMBER

Scenario	Case	Path number		
		M_1	M_2 (X dB)	
			20 dB	30 dB
Indoor office	LOS, horn	11	1.5	6
	LOS, dipole	8	4	9
	NLOS, dipole	10	8	13

Different thresholds are set when we use M_2 to extract the paths will result in different results, especially when SNRs have big gaps. We show the results in Table II when X is set to 20 dB and 30 dB, respectively. The result shows that no matter what type of antenna we use, the path number increases with the reduce of threshold. However, the average path numbers measured by dipole antennas are always greater than that measured by horn antennas.

Different measurement spots have different path numbers due to the variation of surrounding propagation environment. Fig. 7 shows the path numbers in different distances in the condition of $X = 20$ dB.

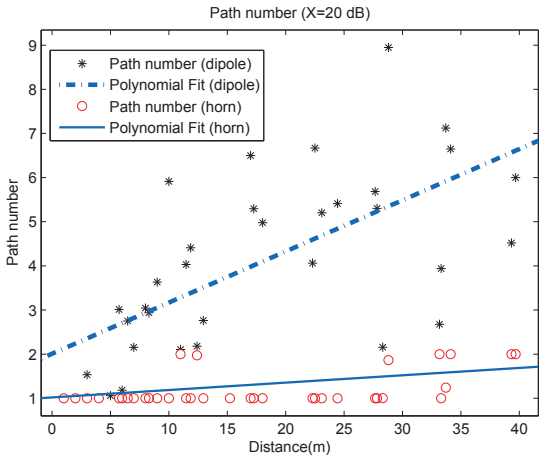

Fig. 7. Path number changes with distance

In conclusion, the path numbers measured by dipole antennas trend to grow with distance increasing, although the change of path number is complex due to the variation of propagation environment. The effective paths measured by horn antennas are rare when we set $X = 20$ dB, so the trend of growth is not obvious. This is because of high gain and high directivity.

In NLOS case, the paths are much richer than that in LOS case, so the path number is greater. Due to lack of direct path, the difference of each path on energy is not too big. Besides,

the total received power is less.

C. Delay

Fig. 8 illustrates the results of rms delay spread in the condition of $X = 20$ dB.

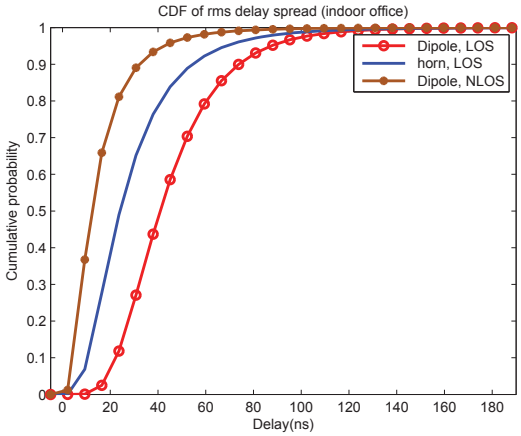

Fig. 8. CDF of rms delay spread

The delay spread measured by dipole antennas is obviously big than that measured by horn antennas. This is due to the directivity of horn antenna, what results in the directions (the value of delay) of measured paths more concentrated.

The value of rms delay spread in NLOS case is bigger than that in LOS case obviously due to more rich paths in space.

Table III shows the results of delay spread results in indoor office scenario.

TABLE III
INDOOR OFFICE DELAY SPREAD RESULTS

Case	RMS Delay Spread[ns]		Mean MED [ns]
	90% CDF	Mean	
LOS,horn	30	21	53
LOS,dipole	52	33	128
NLOS,dipole	73	45	181

Through the above analysis, we find that the rms delay spread results measured by dipole antennas in LOS case are about fifty percent bigger than measured by horn antennas. Besides, in the condition of dipole antenna, the mean RMS delay spread in NLOS case is 12 bigger than in LOS case.

V. CONCLUSION

In this paper, a measurement system main consisting of a vector signal generator, a signal and spectrum analyzer, a pair of horn antennas and a pair of dipole antennas for indoor office channel measurements at 14 GHz is presented. On this basis, propagation characteristics including PDP, path number and rms delay spread were extracted and analyzed. On the one hand, we compared the difference of results measured by horn antennas and dipole antennas in LOS case. On the other hand, we give the main parameters about delay including both of the LOS case and NLOS case.

VI. ACKNOWLEDGMENT

The research is supported by Natural Science and Technology Major Project of the Ministry of Science and Technology and project name is "IMT-2020 Candidate Band Analysis and Evaluation" with 2015ZX03002008, and National 863 Project of the Ministry of Science and Technology and Project name is "High efficiency 5G transmission techniques research" with 2014AA01A705, and National Natural Science Foundation of China and project name is "Theoretical Modeling and Experiment Research of Propagation Channel" with NO.61322110.

REFERENCES

[1] J. Wu, S. Rangan, and H. Zhang, *Green Communications: Theoretical Fundamentals, Algorithms and Applications*. CRC Press, 2012.

[2] J. Zhang, C. Pan, F. Pei, G. Liu, and X. Cheng, "Three-dimensional fading channel models: A survey of elevation angle research," *Communications Magazine, IEEE*, vol. 52, no. 6, pp. 218–226, 2014.

[3] T. S. Rappaport, S. Sun, R. Mayzus, H. Zhao, Y. Azar, K. Wang, G. N. Wong, J. K. Schulz, M. Samimi, and F. Gutierrez, "Millimeter wave mobile communications for 5g cellular: It will work!" *Access, IEEE*, vol. 1, pp. 335–349, 2013.

[4] Z. Pi and F. Khan, "An introduction to millimeter-wave mobile broadband systems," *Communications Magazine, IEEE*, vol. 49, no. 6, pp. 101–107, 2011.

[5] M. Kim, Y. Chang, J.-i. Takada, J. Shen, and Y. Oda, "Spatio-temporal channel characteristics in urban cellular environments at 11 ghz for future high bit-rate communications," in *General Assembly and Scientific Symposium (URSI GASS), 2014 XXXIth URSI*. IEEE, 2014, pp. 1–4.

[6] A. F. Molisch and F. Tufvesson, "Propagation channel models for next-generation wireless communications systems," *IEICE Transactions on Communications*, vol. 97, no. 10, pp. 2022–2034, 2014.

[7] M. Kim, Y. Konishi, Y. Chang, and J.-i. Takada, "Large scale parameters and double-directional characterization of indoor wideband radio multipath channels at 11 ghz," *Antennas and Propagation, IEEE Transactions on*, vol. 62, no. 1, pp. 430–441, 2014.

[8] M. Lei, J. Zhang, T. Lei, and D. Du, "28-ghz indoor channel measurements and analysis of propagation characteristics."

[9] Y. Azar, G. N. Wong, K. Wang, R. Mayzus, J. K. Schulz, H. Zhao, F. Gutierrez, D. Hwang, and T. S. Rappaport, "28 ghz propagation measurements for outdoor cellular communications using steerable beam antennas in new york city," in *Communications (ICC), 2013 IEEE International Conference on*. IEEE, 2013, pp. 5143–5147.

[10] H. Yang, P. F. Smulders, and M. H. Herben, "Channel characteristics and transmission performance for various channel configurations at 60 ghz," *EURASIP Journal on Wireless Communications and Networking*, vol. 2007, no. 1, pp. 43–43, 2007.

[11] T. S. Rappaport, E. Ben-Dor, J. N. Murdock, and Y. Qiao, "38 ghz and 60 ghz angle-dependent propagation for cellular & peer-to-peer wireless communications," in *Communications (ICC), 2012 IEEE International Conference on*, 2012, pp. 4568 – 4573.

[12] W. Kotterman, U. Trautwein, D. Brückner, J. Kunisch, R. S. Thomä *et al.*, "60 ghz time-variant shadowing characterization within an airbus 340," in *Antennas and Propagation (EuCAP), 2010 Proceedings of the Fourth European Conference on*. IEEE, 2010, pp. 1–5.

[13] H. Xu, T. S. Rappaport, R. J. Boyle, and J. H. Schaffner, "Measurements and models for 38-ghz point-to-multipoint radiowave propagation," *Selected Areas in Communications, IEEE Journal on*, vol. 18, no. 3, pp. 310–321, 2000.

[14] C. Gustafson and F. Tufvesson, "Characterization of 60 ghz shadowing by human bodies and simple phantoms," in *Antennas and Propagation (EUCAP), 2012 6th European Conference on*. IEEE, 2012, pp. 473–477.

[15] T. S. Rappaport, F. Gutierrez, E. Ben-Dor, J. N. Murdock, Y. Qiao, J. Tamir *et al.*, "Broadband millimeter-wave propagation measurements and models using adaptive-beam antennas for outdoor urban cellular communications," *Antennas and Propagation, IEEE Transactions on*, vol. 61, no. 4, pp. 1850–1859, 2013.

[16] T. S. Rappaport *et al.*, *Wireless communications: principles and practice*. prentice hall PTR New Jersey, 1996, vol. 2.